2020/11/04
Archive Hash: 9c672cd-D
Archive Date: 2020/10/15

Measurement of B_s^0 and B^+ meson yields in PbPb collisions at $\sqrt{s_{NN}} = 5.02$ TeV

The CMS Collaboration

Abstract

The B_s^0 and B^+ production cross sections are measured in lead-lead (PbPb) collisions at a center-of-mass energy per nucleon pair of 5.02 TeV. The data sample, collected with the CMS detector at the LHC, corresponds to an integrated luminosity of 1.7 nb^{-1}. The mesons are reconstructed in the exclusive decay channels $B_s^0 \to J/\psi\,\phi(1020)$ and $B^+ \to J/\psi\,K^+$ where the J/ψ ($\phi(1020)$) meson is $\mu^+\mu^-$ (K^+K^-) The B_s^0 meson is observed with a statistical significance in excess of fivef standard deviations for the first time in nucleus-nucleus collisions. The measurements are performed as a function of the transverse momentum of the B mesons, in the interval 7–50 GeV/c, and of the PbPb collision centrality. The ratio of production yields of B_s^0 and B^+ is also presented.

1 Introduction

Relativistic heavy ion collisions allow the study of quantum chromodynamics (QCD) at high energy density and temperature. Under such extreme conditions, a state in which the quarks and gluons are the relevant degrees of freedom, the quark-gluon plasma (QGP) [1, 2], is predicted by the lattice QCD calculations [3]. Multiple probes are necessary for characterizing the properties of the QGP medium created in heavy ion collisions and for thereby gaining further understanding of the underlying processes. Heavy quarks are abundantly produced at the CERN Large Hadron Collider (LHC), and their exploration has the potential of providing novel insights in perturbative QCD calculations [4] and as probes of the QGP [5]. Hard-scattered partons lose energy by means of elastic collisions and medium-induced gluon radiation [4, 6–9] as they traverse the QGP. The study of the phenomenon of parton energy loss can provide insights into the energy density and diffusion properties of the QGP. The measurement of exclusive beauty and charm hadron decays facilitates added precision and allows the study of flavor and mass dependence for such processes. Although precise heavy flavor data became available at the BNL RHIC and the LHC, there are still large theoretical uncertainties on the hadronization of heavy quarks in the presence of QGP [10]. Therefore, a more precise understanding of the hadronization mechanism using fully reconstructed heavy-flavor mesons is needed for the extraction of transport properties of the QGP using heavy quarks.

An enhancement in strangeness content [11–17] is expected when the medium temperature lies above the strange quark mass [18]. Complementary to the direct reconstruction of (light-quark) strange mesons and baryons, strangeness content enhancement in the QGP may be further probed using heavy quarks. Through a quark-recombination mechanism [4, 19–22], a corresponding yield enhancement of hadrons containing strangeness is expected relative to corresponding hadrons that do not contain strange quarks. Hints of the presence of such recombination processes also for heavy mesons were recently detected in the open-charm [23] and open-beauty [24] sectors at the LHC, in lead-lead (PbPb collisions at $\sqrt{s_{\mathrm{NN}}} = 5.02\,\mathrm{TeV}$.

The production of B mesons employing fully reconstructed decay was studied at the LHC in proton-proton (pp) collisions at center-of-mass energies of $\sqrt{s} = 7\,\mathrm{TeV}$ [25–31], 8 TeV [32, 33] and 13 TeV [34] over wide transverse momentum (p_{T}) and rapidity (y) intervals, and in proton-lead (pPb) collisions at a center-of-mass energy per nucleon pair of $\sqrt{s_{\mathrm{NN}}} = 5.02\,\mathrm{TeV}$ [35]. In PbPb collisions, the CMS Collaboration reported results at $\sqrt{s_{\mathrm{NN}}} = 5.02\,\mathrm{TeV}$ for the B^+ [36] and $\mathrm{B}_{\mathrm{s}}^0$ [24] mesons. In this Letter, we extend these results, employing the PbPb data set collected at the end of 2018, a sample larger by about a factor of three compared to the first measurement with 2015 data, resulting in increased statistical precision and significance.

The B mesons are reconstructed via the exclusive decay channels $\mathrm{B}_{\mathrm{s}}^0 \to \mathrm{J}/\psi\phi(1020)$ and $\mathrm{B}^+ \to \mathrm{J}/\psi\mathrm{K}^+$, with $\mathrm{J}/\psi \to \mu^+\mu^-$ and $\phi(1020) \to \mathrm{K}^+\mathrm{K}^-$. Throughout the paper, unless otherwise specified, the y and p_{T} variables given are those of the B mesons, and charge-conjugated states are assumed. The production cross sections of the $\mathrm{B}_{\mathrm{s}}^0$ and B^+ mesons in PbPb collisions at $\sqrt{s_{\mathrm{NN}}} = 5.02\,\mathrm{TeV}$ and their ratios are reported here, using a data set corresponding to an integrated luminosity of $1.7\,\mathrm{nb}^{-1}$ collected by the CMS experiment. The measurements are performed as functions of the meson p_{T} and of the PbPb collision centrality (which characterizes the degree of overlap of the two lead nuclei).

2 Experimental apparatus and data sample

The central feature of the CMS detector is a superconducting solenoid, which provides a magnetic field of 3.8 T. Within the solenoid volume are a silicon tracker that measures charged parti-

cles in the pseudorapidity range $|\eta| < 2.5$, a lead tungstate crystal electromagnetic calorimeter, and a brass and scintillator hadron calorimeter. For charged particles of $1 < p_T < 10\,\text{GeV}/c$ and $|\eta| < 1.4$, the track resolutions are typically 1.5% in p_T and 25–90 (45–150) μm in the transverse (longitudinal) impact parameter [37]. Muons are measured in the range $|\eta| < 2.4$, with detection planes made using three technologies: drift tubes, cathode strip chambers, and resistive-plate chambers. The muon reconstruction algorithm starts by finding tracks in the muon detectors, which are then fitted together with tracks reconstructed in the silicon tracker to form "global muons". Matching muons to tracks measured in the silicon tracker results in a relative p_T resolution for muons with $20 < p_T < 100\,\text{GeV}/c$ of 1.3–2.0% in the barrel and better than 6% in the endcaps. The hadron forward (HF) calorimeter uses steel as an absorber and quartz fibers as the sensitive material. The two halves of the HF are located 11.2 m away from the interaction point, one on each end, providing together coverage in the range $3.0 < |\eta| < 5.2$. In this analysis, the HF information is used to select PbPb collision events and to define their centrality class. Centrality, defined as the fraction of the total inelastic hadronic cross section with 0% representing collisions with the largest overlap of the two nuclei, is determined experimentally using the total energy in both HF calorimeters [38]. Events are filtered using a two-tiered trigger system [39]. The first level (L1), composed of custom hardware processors, uses information from the calorimeters and muon detectors to select events within a fixed time interval of less than 4 μs. The second level, known as the high-level trigger (HLT), consists of a farm of processors running a version of the full event reconstruction software optimized for fast processing. A detailed description of the CMS experiment and coordinate system can be found in Ref. [40].

Several Monte Carlo (MC) simulated event samples are used to evaluate background components, signal efficiencies and detector acceptance corrections. The simulations include samples containing only the B meson decay channels being measured, and samples with prompt and nonprompt J/ψ mesons (from b hadron decays which are different from the reconstruction channels used in the analysis, but recorded as candidates) mesons. Proton-proton simulated collisions are generated with PYTHIA8 v212 [41] tune CUETP8M1 [42] and propagated through the CMS detector model using the GEANT4 package [43]. The decay of the B mesons is modeled with EVTGEN 1.3.0 [44], and final-state photon radiation is simulated with PHOTOS 2.0 [45]. Each PYTHIA8 event is embedded into a PbPb collision event generated with HYDJET 1.8 [46], which is tuned to reproduce global event properties, such as the charged-hadron p_T spectrum and particle multiplicity.

The PbPb events were collected with a trigger algorithm requiring the presence of two muon candidates, with no explicit momentum threshold, in coincidence with lead bunches crossing in the interaction point, and with an invariant mass within $1 < m(\mu\mu) < 5\,\text{GeV}/c^2$. One of the trigger-level muons is reconstructed using information both from the muon detectors and the inner tracker, while for the other only information from the muon detectors is required. For the offline analysis, events have to pass a set of selection criteria designed to reject events from background processes (beam-gas collisions and beam scraping events) as described in Ref. [47]. Events are required to have at least one reconstructed primary interaction vertex, formed by two or more tracks, with a distance from the center of the nominal interaction region of less than 15 cm along the beam axis. The shapes of the clusters in the pixel detector must be compatible with those expected from particles produced by a PbPb collision [48]. In order to select inelastic hadronic collisions, the PbPb events are also required to have at least two towers in each of the HF detectors with energy deposits of more than 4 GeV per tower. The combined efficiency for this event selection, including the remaining non-hadronic contamination, is (98 ± 1)%. Only events with centrality 0–90% are selected. Collision centrality

bins are given in percentage ranges, with the 0–90% bin corresponding to the 90% fraction of the collisions having the largest overlap of the two nuclei. The PbPb sample corresponds to an integrated luminosity of approximately $1.7\,\mathrm{nb}^{-1}$. This value is indicative only, as the PbPb yield is normalized by the total number of minimum bias events sampled, $N_{\mathrm{MB}} = 11.8 \times 10^9$.

3 Candidate selection and signal extraction

Muon candidates are selected within kinematic constraints that ensure that their reconstruction efficiency stays above 10%. These limits are $p_{\mathrm{T}}^{\mu} > 3.5\,\mathrm{GeV}/c$ for $|\eta^{\mu}| < 1.2$, $p_{\mathrm{T}}^{\mu} > 1.5\,\mathrm{GeV}/c$ for $2.1 < |\eta^{\mu}| < 2.4$, and $p_{\mathrm{T}}^{\mu} > (5.47 - 1.89|\eta^{\mu}|)\,\mathrm{GeV}/c$ in the $1.2 < |\eta^{\mu}| < 2.1$ region. The muons are also required to match the trigger-level muons candidates and to pass selection criteria optimized for low p_{T} [49].

Two muons of opposite charge, with an invariant mass within $\pm 150\,\mathrm{MeV}/c^2$ of the world-average J/ψ meson mass [50], are selected to reconstruct a J/ψ candidate, with a mass resolution of typically 15–30 MeV/c^2, depending on the dimuon rapidity and p_{T}. The muon pairs are fitted with a common vertex constraint and are kept if the p-value of the χ^2 of the fit is greater than 1%, thus lowering the background from charm and beauty hadron semileptonic decays. Similarly, the $\phi(1020)$ meson candidates are formed with a common vertex constraint between two oppositely charged tracks with $p_{\mathrm{T}} > 300\,\mathrm{MeV}/c$, both required to pass standard selections described in Ref. [47]. The invariant mass, assuming the world-average charged kaon mass [50] for the 2 tracks, with a resolution of $\sim$3.9 MeV/c^2, is required to be within $15\,\mathrm{MeV}/c^2$ of the world-average $\phi(1020)$ meson mass [50].

The $\mathrm{B_s^0}$ ($\mathrm{B^+}$) meson candidates are constructed by combining a J/ψ candidate with a $\phi(1020)$ (track) candidate, and requiring that they originate from a common vertex. In the kinematic vertex fit to the dimuon plus two-track (track) system, the track(s) are assigned the mass of the charged kaon, and the invariant mass of muon pair is constrained to the nominal J/ψ meson mass [50]. The B candidate selections are performed via multivariate discriminators, based on a boosted decision tree (BDT) method [51]. The selection is optimized separately for each meson, as well as each individual bin of p_{T}. The discriminating variables employed include: the χ^2 probability of their decay vertex (the probability for the muon tracks from the J/ψ meson decay and the other charged-particle track(s) to originate from a common vertex), the decay length (normalized by its uncertainty), the pointing angle (the angle between the line segment connecting the primary and decay vertices and the momentum vector of the B meson), the cosine value of the angle between B mesons displacements and momenta in the transverse plane, the two-dimensional (2D) distance between the primary and decay vertices of their daughter tracks (normalized by their uncertainties), and the p_{T} of the daughter charged-particle track(s). For the $\mathrm{B_s^0}$ meson, two additional selection variables are used: the distance along the z-direction between the primary vertex and the decay vertex (normalized by its uncertainty), as well as the absolute difference between the reconstructed $\phi(1020)$ meson invariant mass and its nominal value.

The BDT training is performed employing simulated B signal samples, and background samples taken from data sidebands (candidates with the invariant mass 0.15–0.35 GeV/c^2 away from the B meson nominal mass [50]). The signal samples are scaled to the number of B candidates predicted by the fixed-to-next-to-the-leading order (FONLL) calculations [52–54] normalized to the integrated luminosity of the analyzed data sample.

The raw B meson signal yields are extracted using an extended unbinned maximum likelihood fit to the invariant mass spectra. The signal shape is modeled by a sum of two Gaussian func-

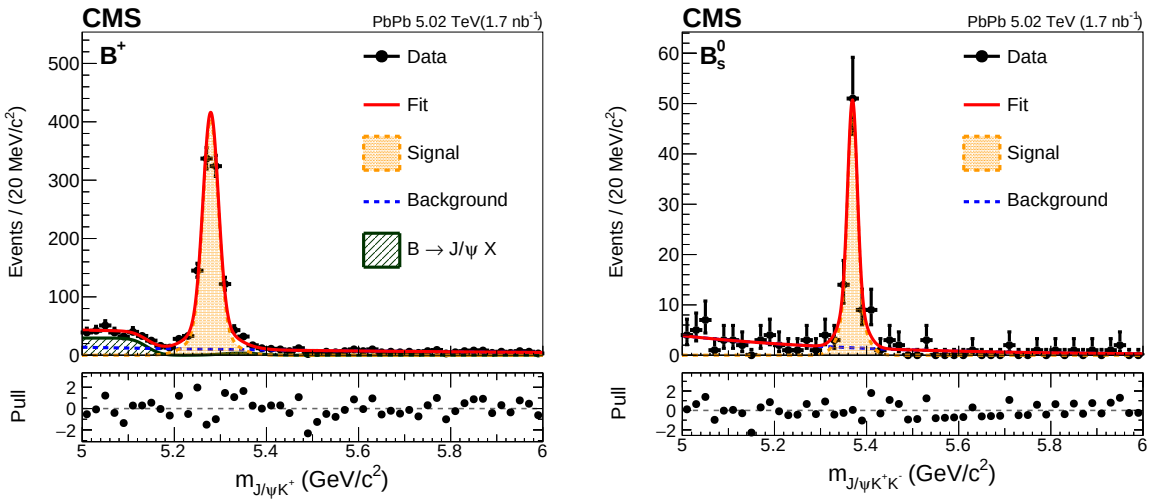

Figure 1: Invariant mass distributions of B^+ (left) and B_s^0 (right) candidates, for event centrality in the range 0–90%. The lower panels show the pulls, obtained as the difference between the data points and the fit result, divided by the uncertainty in data.

tions, with parameters determined from MC simulation, except for the common mean and the overall signal yield that are free parameters of the fit. The combinatorial background, from uncorrelated combinations of J/ψ candidates with extra particles, gives rise to a falling contribution in the invariant mass spectrum which is modeled by an exponential function. An additional background source can arise from possible contamination from other b hadron decays. For the B^+ spectrum, partially reconstructed B decays, such as $B^0 \to J/\psi\, K^{*0} \to \mu^+\mu^- K^+\pi^-$, lead to a heightened background in the invariant mass region below 5.2 GeV/c^2. The decay $B^+ \to J/\psi\pi^+$, where the pion is misidentified as a kaon, results in a small peaking structure under the signal peak. Such partially and misreconstructed B hadron components are modeled from simulation, via an error function and a Gaussian function, respectively; both shapes and the normalization of the Gaussian function (relative to the signal) are fixed in the fit to the data. For the B_s^0 meson case, such background contributions are found to be negligible, as a consequence of the tight selection on the mass of the $\phi(1020)$ candidate. The results of the fits to the invariant mass distributions are shown in Fig. 1.

The statistical significance of the B meson signals is estimated from the ratio of likelihoods obtained by fitting the data with the full model and the background-only model. Estimates obtained by this means well exceed 10 standard deviations for both mesons. This is the first observation of the B_s^0 signal in heavy-ion collisions.

4 Production yields

For each B meson, the production yield is computed in each p_T interval according to

$$\frac{1}{T_{AA}}\frac{dN}{dp_T} = \frac{1}{2\,\mathcal{B}\,N_{MB}\,T_{AA}}\frac{N_{obs}(p_T)}{\Delta p_T} \times \left\langle \frac{1}{\alpha(p_T,y)\times\epsilon(p_T,y)} \right\rangle, \quad (1)$$

where N_{obs} denotes the raw signal yield, extracted in each p_T interval of width Δp_T. The factor 1/2 accounts for the fact that the raw yield is measured for particles and antiparticles added together while the production yield is given for one species only, and $\mathcal{B}$ stands for the branching fraction of the corresponding decay chain. N_{MB} is the number of minimum bias events and

$T_{\rm AA}$ is the nuclear overlap function [55]. The $T_{\rm AA}$ is equal to the number of nucleon-nucleon (NN) binary collisions divided by the NN total inelastic cross section, and it can be interpreted as the NN-equivalent integrated luminosity per heavy ion collision. The $T_{\rm AA}$ value for inclusive PbPb collisions at $\sqrt{s_{\rm NN}} = 5.02\,\text{TeV}$ is $(5.6 \pm 0.2)\,\text{mb}^{-1}$ as estimated from an MC Glauber model [55], implemented in the TGLAUBERMC v3.2 software package [56]. The measurement is performed in a similar fashion as a function of the PbPb collision centrality. The centrality class is represented as the average number of participating nucleons, $\langle N_{\rm part}\rangle$; the latter, determined using the above Glauber model, is highly correlated with the impact parameter of the collision.

The acceptance and the efficiency factors, the last term in Eq. (1), are obtained employing 2D fine-grained maps of the acceptance $\alpha(p_{\rm T}, y)$ and the efficiency $\epsilon(p_{\rm T}, y)$. These maps are determined from MC simulation samples of B meson signal events, generated within the analysis fiducial region given by: $|y| < 1.5,\ p_{\rm T} > 10\,\text{GeV}/c; 1.5 < |y| < 2.4,\ 7 < p_{\rm T} < 50\,\text{GeV}/c$. The acceptance corresponds to the fraction of generated events passing the muon and kaon selection thresholds specified in Section 3, while the efficiency is determined as the fraction of accepted events that pass the full analysis selection criteria, including the trigger. The maps are used to determine the $1/(\alpha \times \epsilon)$ value for each B candidate in data, based on the kinematics $(p_{\rm T}, y)$ of the candidates, and the corresponding average $\langle 1/(\alpha \times \epsilon)\rangle$ obtained for the candidates within a $160\,\text{MeV}/c^2$ window centered on the B meson's world-average mass. The MC-derived efficiency maps are corrected by data/MC scale factors for the muon reconstruction and trigger efficiencies, which are obtained applying the "tag-and-probe" method using the J/ψ resonance [57].

5 Systematic uncertainties

The cross section measurements are affected by several sources of systematic uncertainties arising from the signal extraction, acceptance and efficiency, $\mathcal{B}$, $N_{\rm MB}$, and $T_{\rm AA}$ determinations.

The uncertainty from the signal and background modeling is evaluated by considering the following fit variations: (i) using low-order polynomials for describing the combinatorial background, (ii) using a sum of three Gaussian functions with a common mean for alternatively describing the signal, (iii) varying the widths of the signal double-Gaussian function by 10% (to account for possible mismatches in mass resolution between simulation and data), and (iv) fixing the common Gaussian mean to its MC simulation value. The maximum of the signal variations and the maximum of the background variations are added in quadrature as the systematic uncertainty from fit modeling. The range of the modeling uncertainties is 1.2 - 6.4% for $\rm B_s^0$ and 2.5 - 4.5% for B

The systematic uncertainties associated with the limited size of the MC simulation samples are obtained by re-computing the 2D fine-grained $\alpha(p_{\rm T}, y) \times \epsilon(p_{\rm T}, y)$ maps and the corresponding $\langle 1/(\alpha \times \epsilon)\rangle$ averages over the data sample. The statistical uncertainties from the MC-derived acceptance$\times$efficiency are propagated by generating 10000 2D maps (per bin in the differential measurement), where each entry is obtained by randomly sampling the $\alpha \times \epsilon$ values from Gaussian distributions with widths given by the statistical uncertainty. The resulting systematic uncertainties are obtained as the width of the $\langle 1/(\alpha \times \epsilon\rangle)$ distribution from the alternative 2D maps. The range of the MC event count uncertainties is 2.4 - 27.6% for $\rm B_s^0$ and 1.9 - 9.2% for B

The efficiency and acceptance determinations, based on MC simulation, are further affected by potential disagreements between data and MC . The signal MC simulation is validated against data by inspecting the distributions of the variables employed in the selection. The signal

Table 1: Summary of systematic uncertainties in the production cross section measurements for B^+ and B_s^0 mesons for centrality ranges 0-30%, 30–90%, and 0–90%. The measurements are performed in the B meson kinematic region given by $10 < p_T < 50\,\text{GeV}/c$ and $|y| < 2.4$. The relative uncertainty values are shown, in percentage.

	B^+			B_s^0		
Centrality class	0–30%	30–90%	0–90%	0–30%	30–90%	0–90%
Muon efficiency	$^{+3.2}_{-3.0}$	$^{+3.1}_{-2.9}$	$^{+3.1}_{-2.9}$	$^{+3.8}_{-3.5}$	$^{+3.2}_{-3.0}$	$^{+3.6}_{-3.3}$
Data/MC agreement	13	8.0	11	2.6	3.2	2.7
MC sample size	3.3	2.3	2.5	7.2	2.4	4.7
PDF variation	2.5	2.8	2.6	2.5	3.2	2.3
Tracking efficiency	5.0	5.0	5.0	10	10	10
T_{AA}	2.0	3.6	2.2	2.00	3.6	2.2
N_{MB}(event selection)	1.3	1.2	1.2	1.4	1.2	1.2
Branching fraction		2.8			7.6	

distributions are extracted from the data employing the sPlot method [58], using the mass of the B-meson candidates as discriminating variable, and are also cross-checked with a simple sideband-subtraction method. In particular, the sPlot-derived signal distributions for the BDT score are retrieved from the data, along with the corresponding data/MC ratios. These ratios are in turn used to re-weight the MC simulation, and the resulting deviation in the $\langle 1/(\alpha\times\epsilon)\rangle$ factors are assigned as systematic uncertainties. This procedure is employed using the higher-yield channel, namely the B^+. For the B_s^0 meson, the limited size of the data sample yields results that are compatible between data and simulation, within the statistical uncertainties. As such, the B^+ channel is used as the calibration mode for the B_s^0 channel. A procedure identical to that described above, applied to the B^+ sample, is employed but using only tracking related variables. The systematic uncertainty for the B_s^0 corresponds to that evaluated for the B^+ and further taking the maximum of the deviation determined from tracking related variables to account for the presence of an extra track in the B_s^0 channel..

The uncertainty in the efficiency of the muon trigger, reconstruction, and identification is evaluated using a tag-and-probe technique using the J/ψ meson in data [57]. The derived data/MC scale factors are employed in the determination of the nominal $\alpha\times\epsilon$ 2D maps, while the associated uncertainties are propagated as systematic uncertainty in the $\langle 1/(\alpha\times\epsilon)\rangle$ factors. The difference in the track reconstruction efficiency in data and simulation was estimated by comparing 3-prong and 5-prong D^* decays, $D^* \to K\pi\pi(\pi\pi)$ [47]. This results in 5% (10%) uncertainty in the efficiency determination for the B^+ (B_s^0) decay for involving one (two) kaon(s).

The determination of the $\langle 1/(\alpha\times\epsilon)\rangle$ factors, for each analysis bin, involves averaging over the data. In order to reflect this statistical effect, the overall statistical uncertainty from the PbPb data is calculated using a bootstrap method [59], where data events are resampled 1000 times with replacement. The corrected yield is re-determined for each bootstrap sample, and the spread of its distribution is assigned as the statistical uncertainty.

Various consistency checks of the analysis procedure have been performed, which do not result in additional systematic uncertainties. The consistency of the fitting procedure was verified by generating and fitting pseudo-experiments using the likelihood model and parameters employed for fitting the data. Pull distributions show random behavior consistent with unit

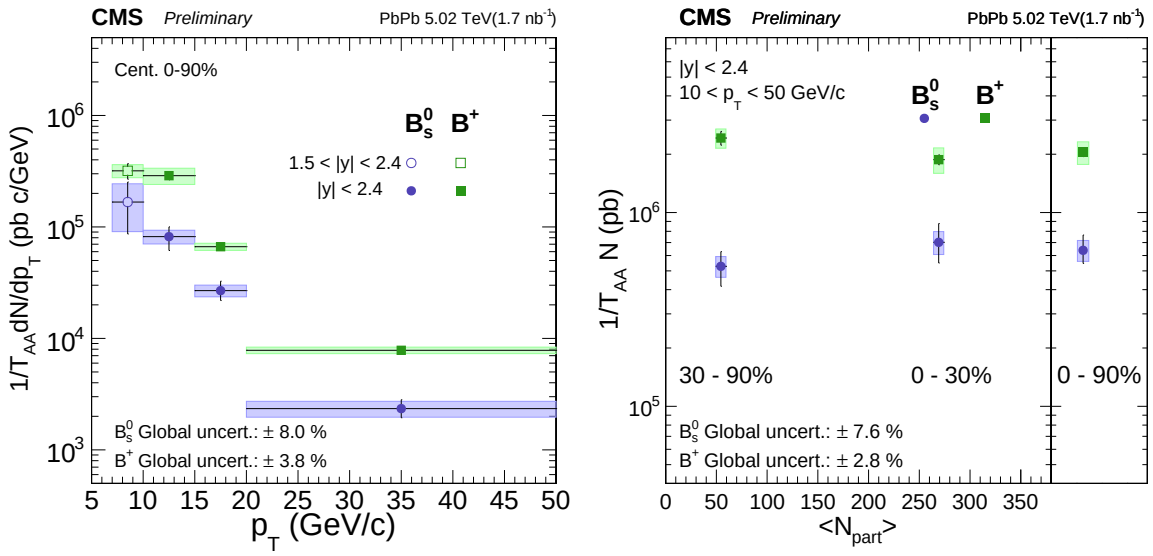

Figure 2: The acceptance- and efficiency-corrected yields for the B^+ and B_s^0 mesons, scaled by T_{AA} and N_{MB} in PbPb collisions at $\sqrt{s_{NN}} = 5.02\,\text{TeV}$. The results are shown as a function of the meson p_T (left), and of the event centrality (right), where the rightmost panel indicates the centrality-integrated result. The vertical bars (boxes) correspond to statistical (systematic) uncertainties. The global systematic uncertainty comprises the uncertainties in T_{AA}, N_{MB}, $\mathcal{B}$ (left) and $\mathcal{B}$ (right).

Gaussians. A consistency check was performed using MC simulation, where the signal yields are extracted with the fitting procedure and the acceptance and efficiency corrections applied, thus retrieving the generated yields. Potential biases in the acceptance and efficiency calculations associated with the shape of the B mesons kinematic distributions from simulation were probed by re-weighting the PYTHIA simulation according to varied p_T shapes and recomputing the factors $\langle 1/(\alpha\times\epsilon)\rangle$. Such deviations were found to be negligible. This confirmed independence from the MC is expected in view of the fine-grained 2D $\alpha\times\epsilon$ MC maps and the $\langle 1/(\alpha\times\epsilon)\rangle$ averaging based on data, and further attests to the robustness of the analysis procedure. The effect of background contamination in the averaging procedure was studied employing the sPlot method and was found to be negligible.

The systematic uncertainties in the Glauber model normalization factor (T_{AA}) are derived from propagating the uncertainties in the event selection efficiency, and in the nuclear radius, skin depth, and minimum distance between nucleons in the Pb nucleus parameters of the Glauber model [47]. The uncertainties associated with the branching fraction of the decay chains $\mathcal{B}$ are obtained from Ref. [50]. The $\mathcal{B}$ factor is common to all bins in the cross section measurements, as is the case also of T_{AA} and N_{MB} in the p_T-differential results; the corresponding uncertainties are denoted global uncertainties. The total systematic uncertainties in the cross section measurement are computed as the sum in quadrature of the different contributions mentioned above, which are summarized in Table 1.

6 Yield ratio

The differential production yields for B_s^0 and B^+ mesons in PbPb collisions, Eq. 1, are presented in Fig. 2 as functions of the mesons p_T (left) and event centrality (right).

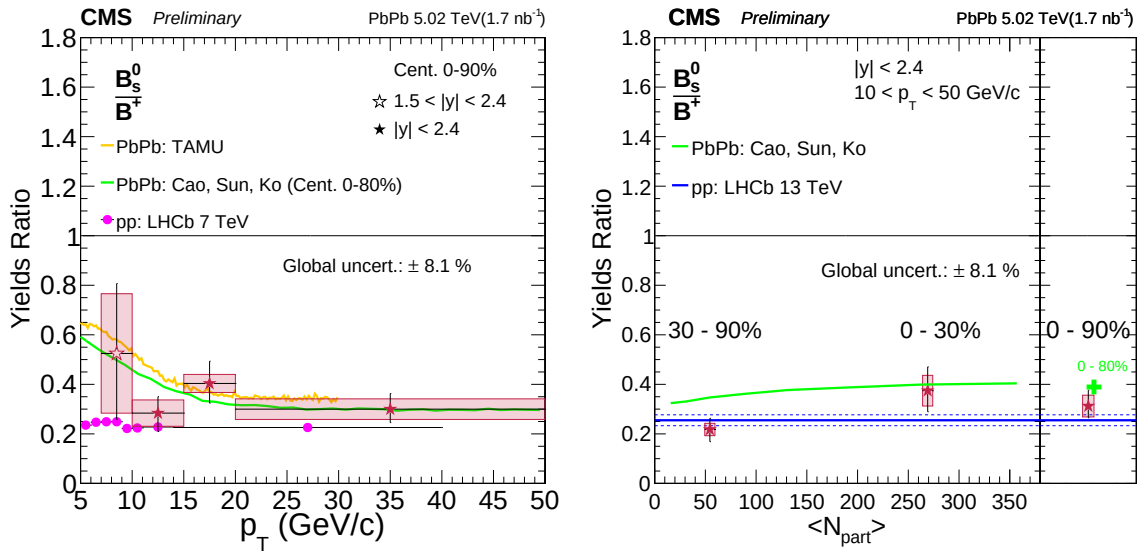

Figure 3: The ratio of production yields between B_s^0 and B^+ mesons. (left) The ratio dependence on the meson p_T; a prediction from the TAMU transport model [60], and the f_s/f_u p_T dependence by LHCb [61] in pp collisions at 7 TeV are also displayed. (right) The ratio dependence on the collision centrality; the average f_s/f_u result obtained in pp 7 TeV collisions by LHCb [61] is also displayed as a horizontal bar; the rightmost panel shows the centrality-integrated measurement. The vertical bars (boxes) correspond to statistical (systematic) uncertainties. The global systematic uncertainty on the yields ratio corresponds to the decay branching fractions $\mathcal{B}$.

The ratio of production yields of the B_s^0 and B^+ mesons is formed as

$$R = \frac{N^{B_s^0}}{N^{B^+}} = \frac{N_{obs}^{B_s^0}}{N_{obs}^{B^+}} \frac{\mathcal{B}^{B^+}}{\mathcal{B}^{B_s^0}} \frac{\langle 1/(\alpha^{B_s^0} \times \epsilon^{B_s^0}) \rangle}{\langle 1/(\alpha^{B^+} \times \epsilon^{B^+}) \rangle}. \quad (2)$$

The terms associated with the size of the data sample (T_{AA}, N_{MB}) cancel in the ratio R. Correlated systematic uncertainties associated with the efficiency determination are partially reduced. For the tracking efficiency, a 5% uncertainty is assigned, following from the different number of hadron tracks in the two decays. Muon efficiency uncertainties from tag-and-probe are determined by varying coherently the efficiency factors in the numerator and denominator within the corresponding uncertainties. For the determination of uncertainties related to data/MC comparisons, an identical procedure to that used for the cross sections is employed but using only tracking related variables, using the B^+ channel. The dominant uncertainty arises from data/MC agreement and a limited MC sample size. The R ratio results are shown in Fig. 3 as functions of the mesons p_T (left) and event centrality (right).

The p_T dependence of the ratio R is compared to a transport model (TAMU) based on a Langevin equation that includes collisional energy loss and heavy-quark diffusion in the medium [60]. The prediction accounts for recombination contributions to B_s^0 meson yield, which are expected to be more significant at low p_T. The ratio of the B_s^0 and B^+ fragmentation fractions has been determined by LHCb to be $f_s/f_u = 0.244 \pm 0.012$ [61] in pp collisions at 13 TeV, for B mesons transverse momenta from 4 to 25 GeV/c and pseudorapidity 2 to 5. While no rapidity dependence of the ratio on rapidity has been reported, a decrease with p_T has been observed therein. The results are compatible with both the model prediction for PbPb collisions and the pp reference results. However, no significant p_T dependence can be established with the precision

allowed by the current data. The results, while compatible, tend to lie systematically above the pp 7 TeV reference. While the central value of R in the high-centrality bin lies above that of the low-centrality bin, the results are compatible within the combined statistical and systematic uncertainty, and no significant dependence on centrality can be inferred within the precision allowed by the data set. These results are compatible with the ratio of R_{AA} reported earlier by the CMS Collaboration [24]. However more PbPb data will be needed. Furthermore, an increase of the ratio R with pp collision energy has been recently reported by LHCb [61], which points to the need of a more complete understanding of the pp reference.

7 Summary

The production yields of B_s^0 and B^+ mesons, scaled by the nuclear overlap function T_{AA} and the number of minimum biased events N_{MB}, in PbPb collisions at a center-of-mass energy of 5.02 TeV per nucleon pair are presented as a function of the meson transverse momenta and event centrality. The B mesons are studied with the CMS detector at the LHC via the reconstruction of the exclusive hadronic decay channels $\mathrm{B}_\mathrm{s}^0 \to \mathrm{J}/\psi\phi(1020) \to \mu^+\mu^-\mathrm{K}^+\mathrm{K}^-$ and $\mathrm{B}^+ \to \mathrm{J}/\psi\mathrm{K}^+ \to \mu^+\mu^-\mathrm{K}^+$. The measurements are performed within the B mesons fiducial region given by $p_{\mathrm{T}} > 10\,\mathrm{GeV}/c$ for $|y| < 1.5$ and $7 < p_{\mathrm{T}} < 50\,\mathrm{GeV}/c$ for $1.5 < |y| < 2.4$. The ratio of production yields for B_s^0 and B^+ in PbPb collisions is found to be statistically compatible with the corresponding fragmentation fraction ratio, f_s/f_u. These results extend, and are compatible with, those previously reported by the CMS Collaboration [24, 36], and employ a three-fold larger PbPb data sample. The further investigation of possible hints of an enhancement of the ratio in PbPb relative to pp collisions will benefit from more precise PbPb and pp reference data taken at the same collision energy. The first observation of the B_s^0 meson in nucleus-nucleus collisions, with a statistical significance surpassing five standard deviations, is attained. The larger PbPb data sets that should be accumulated in upcoming high-luminosity LHC heavy ion runs will provide additional precision and shall help to further characterize the mechanisms of beauty hadronization in heavy ion collisions.

Acknowledgments

We congratulate our colleagues in the CERN accelerator departments for the excellent performance of the LHC and thank the technical and administrative staffs at CERN and at other CMS institutes for their contributions to the success of the CMS effort. In addition, we gratefully acknowledge the computing centers and personnel of the Worldwide LHC Computing Grid for delivering so effectively the computing infrastructure essential to our analyses. Finally, we acknowledge the enduring support for the construction and operation of the LHC and the CMS detector provided by the following funding agencies: BMBWF and FWF (Austria); FNRS and FWO (Belgium); CNPq, CAPES, FAPERJ, FAPERGS, and FAPESP (Brazil); MES (Bulgaria); CERN; CAS, MoST, and NSFC (China); COLCIENCIAS (Colombia); MSES and CSF (Croatia); RPF (Cyprus); SENESCYT (Ecuador); MoER, ERC IUT, and ERDF (Estonia); Academy of Finland, MEC, and HIP (Finland); CEA and CNRS/IN2P3 (France); BMBF, DFG, and HGF (Germany); GSRT (Greece); NKFIA (Hungary); DAE and DST (India); IPM (Iran); SFI (Ireland); INFN (Italy); MSIP and NRF (Republic of Korea); MES (Latvia); LAS (Lithuania); MOE and UM (Malaysia); BUAP, CINVESTAV, CONACYT, LNS, SEP, and UASLP-FAI (Mexico); MOS (Montenegro); MBIE (New Zealand); PAEC (Pakistan); MSHE and NSC (Poland); FCT (Portugal); JINR (Dubna); MON, RosAtom, RAS, RFBR, and NRC KI (Russia); MESTD (Serbia); SEIDI, CPAN, PCTI, and FEDER (Spain); MOSTR (Sri Lanka); Swiss Funding Agencies (Switzerland);

MST (Taipei); ThEPCenter, IPST, STAR, and NSTDA (Thailand); TUBITAK and TAEK (Turkey); NASU and SFFR (Ukraine); STFC (United Kingdom); DOE and NSF (USA).

References

[1] É. V. Shuryak, "Theory of hadronic plasma", *Sov. Phys. JETP* **47** (1978) 212.

[2] J. C. Collins and M. J. Perry, "Superdense matter: neutrons or asymptotically free quarks?", *Phys. Rev. Lett.* **34** (1975) 1353, doi:10.1103/PhysRevLett.34.1353.

[3] F. Karsch and E. Laermann, "Thermodynamics and in-medium hadron properties from lattice QCD", in *Quark-Gluon Plasma III, R. Hwa (ed.)*, 2003. 2003. arXiv:hep-lat/0305025.

[4] A. Andronic et al., "Heavy-flavour and quarkonium production in the LHC era: from proton-proton to heavy-ion collisions", *Eur. Phys. J. C* **76** (2016) 107, doi:10.1140/epjc/s10052-015-3819-5, arXiv:1506.03981.

[5] X. Dong, Y.-J. Lee, and R. Rapp, "Open heavy-flavor production in heavy-ion collisions", arXiv:1903.07709.

[6] J. D. Bjorken, "Energy loss of energetic partons in quark-gluon plasma: possible extinction of high p_{T} jets in hadron-hadron collisions", Fermilab PUB 82-059-THY, 1982.

[7] R. Baier, D. Schiff, and B. G. Zakharov, "Energy loss in perturbative QCD", *Ann. Rev. Nucl. Part. Sci.* **50** (2000) 37, doi:10.1146/annurev.nucl.50.1.37, arXiv:hep-ph/0002198.

[8] CMS Collaboration, "Observation and studies of jet quenching in PbPb collisions at $\sqrt{s_{\mathrm{NN}}} = 2.76$ TeV", *Phys. Rev. C* **84** (2011) 024906, doi:10.1103/PhysRevC.84.024906, arXiv:1102.1957.

[9] ATLAS Collaboration, "Observation of a centrality-dependent dijet asymmetry in lead-lead collisions at $\sqrt{s_{\mathrm{NN}}} = 2.76$ TeV with the ATLAS detector at the LHC", *Phys. Rev. Lett.* **105** (2010) 252303, doi:10.1103/PhysRevLett.105.252303, arXiv:1011.6182.

[10] A. Beraudo et al., "Extraction of heavy-flavor transport coefficients in QCD matter", *Nucl. Phys. A* **979** (2018) 21, doi:10.1016/j.nuclphysa.2018.09.002, arXiv:1803.03824.

[11] ALICE Collaboration, "Enhanced production of multi-strange hadrons in high-multiplicity proton-proton collisions", *Nature Phys.* **13** (2017) 535, doi:10.1038/nphys4111, arXiv:1606.07424.

[12] ALICE Collaboration, "K^0_S and Λ production in Pb-Pb collisions at $\sqrt{s_{NN}}$ = 2.76 TeV", *Phys. Rev. Lett.* **111** (2013) 222301, doi:10.1103/PhysRevLett.111.222301, arXiv:1307.5530.

[13] STAR Collaboration, "Strangeness enhancement in Cu+Cu and Au+Au collisions at $\sqrt{s_{\mathrm{NN}}} = 200$ GeV", *Phys. Rev. Lett.* **108** (2012) 072301, doi:10.1103/PhysRevLett.108.072301, arXiv:1107.2955.

[14] STAR Collaboration, "Energy and system size dependence of phi meson production in Cu+Cu and Au+Au collisions", *Phys. Lett. B* **673** (2009) 183, doi:10.1016/j.physletb.2009.02.037, arXiv:0810.4979.

[15] BRAHMS Collaboration, "Kaon and pion production in central Au+Au collisions at $\sqrt{s_{\rm NN}} = 62.4\,\text{GeV}$", *Phys. Lett. B* **687** (2010) 36, doi:10.1016/j.physletb.2010.02.078, arXiv:0911.2586.

[16] STAR Collaboration, "Collision energy dependence of moments of net-kaon multiplicity distributions at RHIC", *Phys. Lett. B* **785** (2018) 551, doi:10.1016/j.physletb.2018.07.066, arXiv:1709.00773.

[17] PHENIX Collaboration, "ϕ meson production in the forward/backward rapidity region in Cu+Au collisions at $\sqrt{s_{\rm NN}} = 200$ GeV", *Phys. Rev. C* **93** (2016) 024904, doi:10.1103/PhysRevC.93.024904, arXiv:1509.06337.

[18] J. Rafelski and B. Müller, "Strangeness production in the Quark-Gluon Plasma", *Phys. Rev. Lett.* **48** (1982) 1066, doi:10.1103/PhysRevLett.48.1066. [Erratum: doi:10.1103/PhysRevLett.56.2334].

[19] D. Molnar and S. A. Voloshin, "Elliptic flow at large transverse momenta from quark coalescence", *Phys. Rev. Lett.* **91** (2003) 092301, doi:10.1103/PhysRevLett.91.092301, arXiv:nucl-th/0302014.

[20] V. Greco, C. M. Ko, and P. Levai, "Parton coalescence at RHIC", *Phys. Rev. C* **68** (2003) 034904, doi:10.1103/PhysRevC.68.034904, arXiv:nucl-th/0305024.

[21] V. Greco, C. M. Ko, and R. Rapp, "Quark coalescence for charmed mesons in ultrarelativistic heavy ion collisions", *Phys. Lett. B* **595** (2004) 202, doi:10.1016/j.physletb.2004.06.064, arXiv:nucl-th/0312100.

[22] M. He, R. J. Fries, and R. Rapp, "Heavy flavor at the large hadron collider in a strong coupling approach", *Phys. Lett. B* **735** (2014) 445, doi:10.1016/j.physletb.2014.05.050, arXiv:1401.3817.

[23] ALICE Collaboration, "Measurement of $\rm D^0$, $\rm D^+$, $\rm D^{*+}$ and $\rm D_s^+$ production in Pb-Pb collisions at $\sqrt{s_{\rm NN}} = 5.02\,\text{TeV}$", *JHEP* **10** (2018) 174, doi:10.1007/JHEP10(2018)174, arXiv:1804.09083.

[24] CMS Collaboration, "Measurement of $\rm B_s^0$ meson production in pp and PbPb collisions at $\sqrt{s_{\rm NN}} = 5.02\,\text{TeV}$", *Phys. Lett. B* **796** (2019) 168, doi:10.1016/j.physletb.2019.07.014, arXiv:1810.03022.

[25] CMS Collaboration, "Measurement of the $\rm B^+$ production cross section in pp collisions at $\sqrt{s} = 7\,\text{TeV}$", *Phys. Rev. Lett.* **106** (2011) 112001, doi:10.1103/PhysRevLett.106.112001, arXiv:1101.0131.

[26] CMS Collaboration, "Measurement of the $\rm B^0$ production cross section in pp collisions at $\sqrt{s} = 7\,\text{TeV}$", *Phys. Rev. Lett.* **106** (2011) 252001, doi:10.1103/PhysRevLett.106.252001, arXiv:1104.2892.

[27] CMS Collaboration, "Measurement of the $\rm B_s^0$ production cross section with $\rm B_s^0 \to J/\psi\phi$ decays in pp collisions at $\sqrt{s} = 7\,\text{TeV}$", *Phys. Rev. D* **84** (2011) 052008, doi:10.1103/PhysRevD.84.052008, arXiv:1106.4048.

[28] ATLAS Collaboration, "Measurement of the differential cross-section of B^+ meson production in pp collisions at $\sqrt{s} = 7$ TeV at ATLAS", *JHEP* **10** (2013) 042, doi:10.1007/JHEP10(2013)042, arXiv:1307.0126.

[29] LHCb Collaboration, "Measurement of B meson production cross-sections in proton-proton collisions at $\sqrt{s} = 7$ TeV", *JHEP* **08** (2013) 117, doi:10.1007/JHEP08(2013)117, arXiv:1306.3663.

[30] LHCb Collaboration, "Measurement of the $\chi_b(3P)$ mass and of the relative rate of $\chi_{b1}(1P)$ and $\chi_{b2}(1P)$ production", *JHEP* **10** (2014) 88, doi:10.1007/JHEP10(2014)088, arXiv:1409.1408.

[31] LHCb Collaboration, "Measurements of B_c^+ production and mass with the $B_c^+ \to J/\psi\pi^+$ decay", *Phys. Rev. Lett.* **109** (2012) 232001, doi:10.1103/PhysRevLett.109.232001, arXiv:1209.5634.

[32] LHCb Collaboration, "Study of the production of Λ_b^0 and $\overline{B}^0$ hadrons in pp collisions and first measurement of the $\Lambda_b^0 \to J/\psi p K^-$ branching fraction", *Chin. Phys. C* **40** (2016) 011001, doi:10.1088/1674-1137/40/1/011001, arXiv:1509.00292.

[33] LHCb Collaboration, "Measurement of B_c^+ production in proton-proton collisions at $\sqrt{s} = 8$ TeV", *Phys. Rev. Lett.* **114** (2015) 132001, doi:10.1103/PhysRevLett.114.132001, arXiv:1411.2943.

[34] CMS Collaboration, "Measurement of the total and differential inclusive B^+ hadron cross sections in pp collisions at $\sqrt{s} = 13$ TeV", *Phys. Lett. B* **771** (2017) 435, doi:10.1016/j.physletb.2017.05.074, arXiv:1609.00873.

[35] CMS Collaboration, "Study of B meson production in p+Pb collisions at $\sqrt{s_{NN}} = 5.02$ TeV using exclusive hadronic decays", *Phys. Rev. Lett.* **116** (2016) 032301, doi:10.1103/PhysRevLett.116.032301, arXiv:1508.06678.

[36] CMS Collaboration, "Measurement of the $B^{\pm}$ meson nuclear modification factor in Pb-Pb collisions at $\sqrt{s_{NN}} = 5.02$ TeV", *Phys. Rev. Lett.* **119** (2017) 152301, doi:10.1103/PhysRevLett.119.152301, arXiv:1705.04727.

[37] CMS Collaboration, "Description and performance of track and primary-vertex reconstruction with the CMS tracker", *JINST* **9** (2014) P10009, doi:10.1088/1748-0221/9/10/P10009, arXiv:1405.6569.

[38] CMS Collaboration, "Dependence on pseudorapidity and centrality of charged hadron production in PbPb collisions at a nucleon-nucleon centre-of-mass energy of 2.76 TeV", *JHEP* **08** (2011) 141, doi:10.1007/JHEP08(2011)141, arXiv:1107.4800.

[39] CMS Collaboration, "The CMS trigger system", *JINST* **12** (2017) P01020, doi:10.1088/1748-0221/12/01/P01020, arXiv:1609.02366.

[40] CMS Collaboration, "The CMS experiment at the CERN LHC", *JINST* **3** (2008) S08004, doi:10.1088/1748-0221/3/08/S08004.

[41] T. Sjöstrand et al., "An introduction to PYTHIA 8.2", *Comput. Phys. Commun.* **191** (2015) 159, doi:10.1016/j.cpc.2015.01.024, arXiv:1410.3012.

[42] CMS Collaboration, "Event generator tunes obtained from underlying event and multiparton scattering measurements", *Eur. Phys. J. C* **76** (2016) doi:10.1140/epjc/s10052-016-3988-x, arXiv:1512.00815.

[43] J. Allison et al., "Recent developments in Geant4", *Nucl. Instrum. Meth. A* **835** (2016) 186, doi:10.1016/j.nima.2016.06.125.

[44] D. J. Lange, "The EvtGen particle decay simulation package", *Nucl. Instrum. Meth. A* **462** (2001) 152, doi:10.1016/S0168-9002(01)00089-4.

[45] E. Barberio, B. van Eijk, and Z. Was, "PHOTOS: A universal monte carlo for QED radiative corrections in decays", *Comput. Phys. Commun.* **66** (1991) 115, doi:10.1016/0010-4655(91)90012-A.

[46] I. P. Lokhtin and A. M. Snigirev, "A model of jet quenching in ultrarelativistic heavy ion collisions and high-p_{T} hadron spectra at RHIC", *Eur. Phys. J. C* **45** (2006) 211, doi:10.1140/epjc/s2005-02426-3, arXiv:hep-ph/0506189.

[47] CMS Collaboration, "Charged-particle nuclear modification factors in PbPb and pPb collisions at $\sqrt{s_{\mathrm{NN}}} = 5.02\,\mathrm{TeV}$", *JHEP* **04** (2017) 039, doi:10.1007/JHEP04(2017)039, arXiv:1611.01664.

[48] CMS Collaboration, "Transverse momentum and pseudorapidity distributions of charged hadrons in pp collisions at $\sqrt{s} = 0.9$ and 2.76 TeV", *JHEP* **02** (2010) 041, doi:10.1007/JHEP02(2010)041, arXiv:1002.0621.

[49] CMS Collaboration, "Performance of CMS muon reconstruction in pp collision events at $\sqrt{s} = 7\,\mathrm{TeV}$", *JINST* **7** (2012) P10002, doi:10.1088/1748-0221/7/10/P10002, arXiv:1206.4071.

[50] Particle Data Group Collaboration, "Review of particle physics", *Phys. Rev. D* **98** (2018) 030001, doi:10.1103/PhysRevD.98.030001.

[51] H. Voss, A. Höcker, J. Stelzer, and F. Tegenfeldt, "TMVA – the toolkit for multivariate data analysis", in *XIth International Workshop on Advanced Computing and Analysis Techniques in Physics Research (ACAT)*, p. 40. 2009. arXiv:physics/0703039.

[52] M. Cacciari, M. Greco, and P. Nason, "The p_{T} spectrum in heavy-flavour hadroproduction", *JHEP* **05** (1998) 007, doi:10.1088/1126-6708/1998/05/007, arXiv:hep-ph/9803400.

[53] M. Cacciari and P. Nason, "Charm cross sections for the Tevatron Run II", *JHEP* **09** (2003) 006, doi:10.1088/1126-6708/2003/09/006, arXiv:hep-ph/0306212.

[54] M. Cacciari et al., "Theoretical predictions for charm and bottom production at the LHC", *JHEP* **10** (2012) 137, doi:10.1007/JHEP10(2012)137, arXiv:1205.6344.

[55] M. L. Miller, K. Reygers, S. J. Sanders, and P. Steinberg, "Glauber modeling in high-energy nuclear collisions", *Ann. Rev. Nucl. Part. Sci.* **57** (2007) 205, doi:10.1146/annurev.nucl.57.090506.123020, arXiv:nucl-ex/0701025.

[56] C. Loizides, J. Kamin, and D. d'Enterria, "Improved Monte Carlo Glauber predictions at present and future nuclear colliders", *Phys. Rev. C* **97** (2018), no. 5, 054910, doi:10.1103/PhysRevC.97.054910, arXiv:1710.07098. [Erratum: Phys.Rev.C 99, 019901 (2019)].

[57] CMS Collaboration, "Upsilon production cross-section in pp collisions at $\sqrt{s} = 7$ TeV", *Phys. Rev. D* **83** (2011) 112004, doi:10.1103/PhysRevD.83.112004, arXiv:1012.5545.

[58] M. Pivk and F. R. Le Diberder, "SPlot: A Statistical tool to unfold data distributions", *Nucl. Instrum. Meth. A* **555** (2005) 356, doi:10.1016/j.nima.2005.08.106, arXiv:physics/0402083.

[59] B. Efron, "Bootstrap methods: another look at the jackknife", *Ann. Statist.* **7** (1979) 1, doi:10.1214/aos/1176344552.

[60] M. He, R. J. Fries, and R. Rapp, "Heavy flavor at the large hadron collider in a strong coupling approach", *Phys. Lett. B* **735** (2014) 445, doi:10.1016/j.physletb.2014.05.050, arXiv:1401.3817.

[61] LHCb Collaboration, "Measurement of f_s/f_u variation with proton-proton collision energy and B-meson kinematics", *Phys. Rev. Lett.* **124** (2020) 122002, doi:10.1103/PhysRevLett.124.122002, arXiv:1910.09934.